International Journal of Heat and Mass Transfer 55 (2012) 5836–5845

Contents lists available at SciVerse ScienceDirect

International Journal of Heat and Mass Transfer

journal homepage: www.elsevier.com/locate/ijhmt

CFD and correlations of the heat transfer from a wall at constant temperature to an impinging swirling jet

J. Ortega-Casanova

Área de Mecánica de Fluidos, ETS de Ingeniería Industrial, C/Dr. Ortiz Ramos s/n, Universidad de Málaga, 29071 Málaga, Spain

ARTICLE INFO

Article history:
Received 2 August 2011
Accepted 18 May 2012
Available online 27 June 2012

Keywords:
Heat transfer
Turbulent impinging swirling jet
Numerical simulations
Nusselt number correlations

ABSTRACT

Numerical simulations of the impingement of a swirling jet against a heated solid wall at a prescribed temperature are presented in order to propose correlations of the heat transfer coefficients along the heated wall as a function of the jet Reynolds number *Re*, jet swirl intensity S_i, jet average turbulent intensity I_{avg}, and jet to wall spacing *H*. The swirling jet used as boundary condition of the numerical simulations is the one described by Ortega-Casanova et al. [1]. It is created by a experimental nozzle (whose exit diameter is *D*) and with the swirl given to the jet by moving swirl blades: different blade orientations give jets with different swirl intensities. In Ortega-Casanova et al. [1], the jet velocity components (measured by means of a LDA system) just at the nozzle exit and their mathematical models are also presented for seven Reynolds numbers and each nozzle configuration. The LDA measurements show the jet is axisymmetric and highly turbulent. For those reasons, axisymmetric flow and turbulent models are used in the simulations. The same seven Reynolds numbers and three nozzle-to-wall distances are simulated numerically in this work. Taking into account the blade orientations, the Reynolds numbers and the nozzle-to-wall distances, a total of 63 different simulations have been carried out. From them, correlations of the area-weighted average Nusselt number Nu_{avg} and the stagnation point Nusselt number Nu_0 as a function of the dimensionless parameter *Re* (ranging from around 7000 to 20 000), S_i (ranging from around 0.015 to 0.45), I_{avg} (ranging from around 10 to 40%), and H/D (=5, 10 and 30), are proposed. The results presented in Ortega-Casanova [2], where the heat transfer when other blade orientation is studied, have been also taken into account to obtain some of the proposed correlations.

1. Introduction

This work is part of the numerical simulations carried out of the impingement of swirling jets against a heated solid wall in order to study the heat transferred from the wall to the jet. The swirling jets, created by a nozzle with adjustable swirl blades giving five possible nozzle configurations, have been previously measured, by means of a LDA system, and mathematically modeled [1], where the same jets were used as a mechanism for seabed excavation. The heat transfer results of the impinging swirling jets generated by the nozzle with the swirl blades rotated the maximum possible angle were presented in [2], so the results with other blade orientations (actually, three of them) will be discussed here. However, to get some of the final correlations, the results given in [2] will be now included.

The impingement of swirling jets against heated surfaces is frequently used as a tool to increase the heat transfer from the surface just on the stagnation region under the jet and especially on the stagnation point, having the heat transfer a rapid decay in the wall jet region developed along the impinged wall due to the boundary layer development. The extended use of this heat transfer mechanism is due to its possible application in many engineering applications, such as, the heat transfer in gas turbine systems [3]; cooling of electronic devices [4]; heat transfer on vehicle windscreens [5]; cooling of grinding processes [6], among others.

However, not always that a heat transfer-related engineering application must be known, it has to be experimentally mounted and tested, because a preliminary prediction of the heat transfer results could be obtained using mathematical correlations, normally, in terms of the problem governing parameters. In the case of the study presented in this work about the heat transfer from a heated solid wall to an impinging jet, there are many correlations trying to estimate the Nusselt number coefficients along the heated wall as function of, especially, the jet Reynolds number and the nozzle-to-wall distance. Regarding these correlations, Zuckerman and Lior [7] have compiled a large number of them, previously presented by other authors. Specifically, some of them, that will be cited later and whose correlations will be compared with those presented in this paper, are Chan et al. [8] San and Lai

E-mail address: jortega@uma.es

0017-9310/$ - see front matter © 2012 Elsevier Ltd. All rights reserved.
http://dx.doi.org/10.1016/j.ijheatmasstransfer.2012.05.079

[9], Lytle and Webb [10] Mohanty and Tawfek [11], Behnia et al. [12] Merci and Dick [13], Martin [14] Wen and Jang [15], Yan [16],and Tawfek [17]. Most of the correlations derived by previously mentioned authors are for axial (non-swirling) jets created by means of different mechanism, while none has been found by the author of this work for impinging swirling jets, and then with the jet swirl intensity appearing as a dependent parameter in the correlation. Because of those reasons, the Nusselt number now-proposed correlations are completely new: they include the dependence on the jet swirl intensity defined in a non-dimensional way by S_i (see below).

Before presenting the Nusselt number correlations derived from the numerical simulations of the impingement of swirling jets against a heated solid wall, the kind of swirling jets and how they are generated, together with some details of the swirl generator nozzle, are described in Section 2. Some information given in this Section has been extracted from [1], but it is included now for the reader to have a general idea of the jet. After the swirling jet has been presented, a summary of the numerical simulation details related with the solved equations, the turbulent models used, the grid convergence study carried out, the type of boundary conditions, etc., are presented in Section 3. Next, Section 4 is dedicated to describe the different results obtained after the numerical simulations have been carried out. Throughout its three first subsections, the effect of the Reynolds number, the nozzle-to-wall distance and the jet swirl intensity on the Nusselt number along the heated wall will be described. Finally, in the last subsection, different Nusselt number correlations will be proposed in term of the dimensionless parameters governing the problem, included the swirl one. A list of the conclusions of this work will be presented in Section 5.

2. The swirling jet

The swirling jet is created by a nozzle where the azimuthal motion is given to the flow by means of swirl blades with adjustable angles located at the bottom of the nozzle. A detailed description, as well as a 2D view, of the nozzle used to create the swirling jet can be consulted in [1]. Nevertheless, the main part of it, together with the computational domain, is shown if Fig. 1. Once the fluid enters the nozzle, it goes down, moves through the blades and finally exits the nozzle as a swirling jet. The blades can be mounted with five different angles so swirling jets with five different swirl intensities (or swirl parameters, defined below) can be generated for the same flow rate (or Reynolds number, defined below) through the nozzle. When the blades are mounted radially, no swirl is imparted to the jet and the swirl parameter will be practically zero. This blade configuration will be referred in what follows as Case R. However, with the blades rotated the maximum possible angle, the jet will have highest levels of swirl (and then the highest swirl parameters). This configuration will be referred as Case S2. Between Cases R and S2 there are other 3 possible blade orientations, but only the two ones previous to Case S2, namely Cases S0 and S1, will be considered, so that the heat transfer from a heated solid wall due to the impingement of the swirling jets created by the nozzle configurations R, S0 and S1 will be analyzed numerically in this work (Case S2 was studied in [2] and some information given there will be used now). The remaining blade orientation between Cases R and S0 has no interest since the swirl intensity of the generating jets are practically the same as Case R, so it has not been analyzed. Fig. 2 shows a 2-D view of the swirl blades with the 4 most interesting blade orientations.

Once the swirling jet, for a given flow rate Q, is generated, it can be measured by, for instance, a LDA system and then, the average velocity components $\vec{v} = (U, V, W)$ and its fluctuations $\vec{v}' = (u', v', w')$, both in polar (r, θ, z) coordinates, can be obtained.

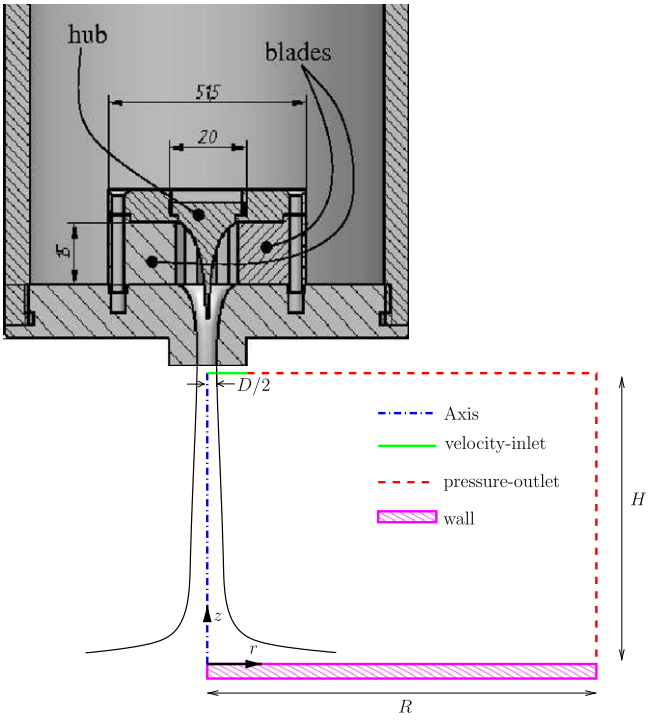

Fig. 1. Part of the nozzle and a sketch of the computation domain (the different boundary conditions used are also included).

Because of the shape of the nozzle exit tube, both the radial average velocity and its fluctuations have been considered negligible and they have not been taken into account to model the swirling jet. The radial variation of the axial an azimuthal velocity components for all Reynolds numbers and blade orientations under study are shown in [1], where the mathematical models used to conveniently fit those experimental profiles are also shown.

Therefore, when a blade orientation is selected, that is, when Case R, S0 or S1 is chosen, the swirling jet will only depend on the flow rate or Reynolds number *Re*, defined as

$$Re = \frac{\rho W_c D}{\mu}, \tag{1}$$

with $W_c = 4Q/(\pi D^2)$ the mean velocity, ρ and μ the density and viscosity of the fluid, respectively, and D the nozzle exit diameter. Thus, jets with different Reynolds numbers will have different swirl intensities. An extended way of quantifying the swirl intensity of a swirling jet is through the integral swirl parameter S_i defined as (see [18])

$$S_i = \frac{\int_0^\infty r^2 WV \, dr}{(D/2)\int_0^\infty r\left(W^2 - \frac{1}{2}V^2\right) dr}. \tag{2}$$

In Fig. 3 is plotted its value as function of the Reynolds number and all Cases: the swirl parameter S_i is practically independent of the Reynolds number ($S_i \approx$ constant) for Cases R, S0 and S1, the ones under study in this work, while for Case S2, S_i depends strongly on the Reynolds number [2].

Regarding the jet turbulence, its modeling is carried out through the relations between the velocity fluctuations $\vec{v}'$ and the turbulent intensity I and its fitting to a Gaussian model [2].

With the corresponding velocity and turbulence mathematical models implicitly presented, the swirling jet can be now used as boundary condition in the numerical simulations.

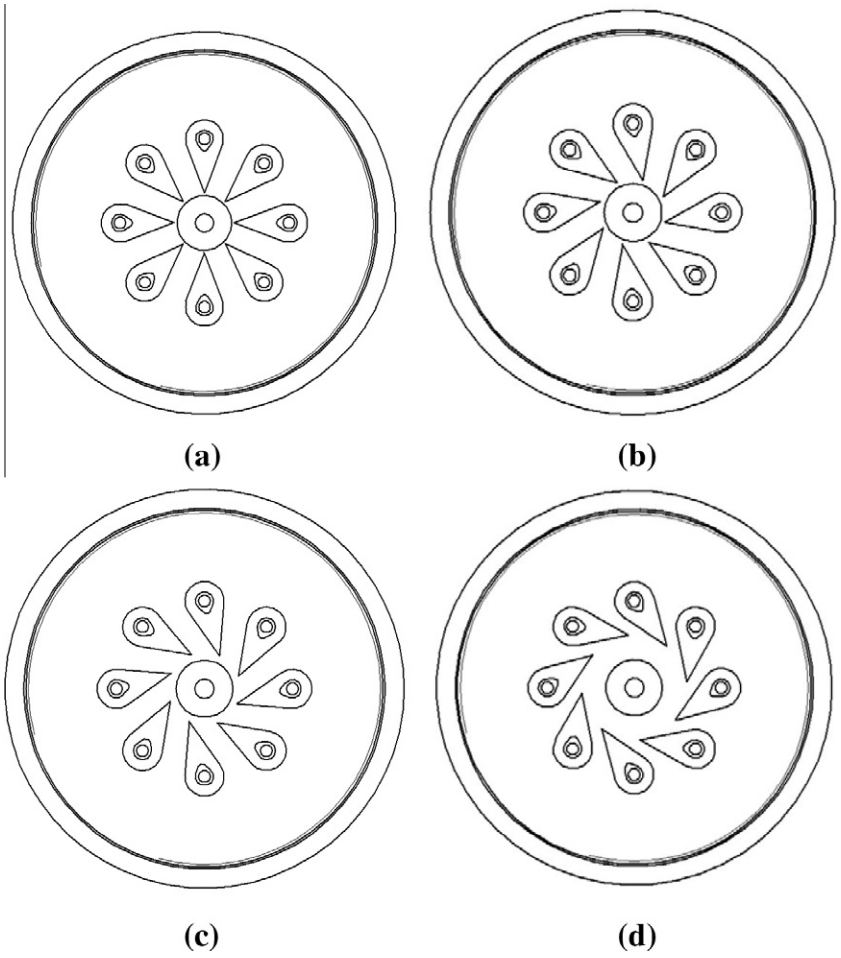

Fig. 2. 2D view of the nozzle blades with four different orientations: (a) Case R, (b) Case S0, (c) Case S1 and (d) Case S2. Configuration (d) was studied in [2].

3. Numerical approach

All characteristics related to the configuration of the numerical simulations are the same than those described in [2]. However, a summary of them will be listed below:

- the commercial code Fluent (version 6.2.16) was used to carry out the numerical simulations;
- the computational geometry, since the velocity profiles at the nozzle exit are axisymmetric, will be axisymmetric, too. It is shown in Fig. 1, where the different boundary conditions used are also shown:
  - the nozzle is located at a distance H above the solid heated wall and its swirling jet is implemented by a "veloc ty-inlet" boundary condition through the velocity component and turbulent intensity models above presented using a Fluent UDF (User Defined Function);
  - the bottom of the geometry represents the heated wall where the fluid will impinge and it is considered as a no-slip surface with radius R at a prescribed temperature and numerically modeled as a "wall" boundary condition (similar results can be obtained when the boundary condition on the solid plate is either a prescribed temperature or heat flux [19]);
  - after the fluid impinges against the wall, it exits the computational domain through either the side or top surfaces, both considered as "pressure-outlet" boundary condition, at the same prescribed constant pressure; and
  - finally, the left line, from the nozzle exit to the wall at the bottom, is considered as an "axis" boundary condition, since it represents the axis of symmetry of the problem.
- the flow under study is considered, not only turbulent and axisymmetric, but also steady with the working fluid (water) incompressible, as in [2];
- the steady Reynolds Averaged Navier–Stokes (RANS) equations are solved numerically to obtain the whole field of any fluid magnitude. They can be written in Cartesian tensor notation as: the continuity equation:

$$\frac{\partial V_i}{\partial x_i} = 0, \tag{3}$$

the momentum equations:

$$\frac{\partial (V_i V_j)}{\partial x_j} = -\frac{1}{\rho}\frac{\partial p}{\partial x_i} + \nu \frac{\partial}{\partial x_j}\left[\frac{\partial V_i}{\partial x_j} + \frac{\partial V_j}{\partial x_i} - \frac{2}{3}\delta_{ij}\frac{\partial V_l}{\partial x_l}\right] + \frac{\partial(-\overline{v_i' v_j'})}{\partial x_j}, \tag{4}$$

and the energy equation:

$$\frac{\partial}{\partial x_i}[V_i(\rho e + p)] = \frac{\partial}{\partial x_j}\left[K_{eff}\frac{\partial T}{\partial x_j}\right] \tag{5}$$

with

$$e = h - \frac{p}{\rho} + \frac{\vec{V}\cdot\vec{V}}{2}. \tag{6}$$

ν is the kinematic viscosity, h is the enthalpy, K is the thermal conductivity and $K_{eff} = K + K_t$ is the effective thermal conductivity

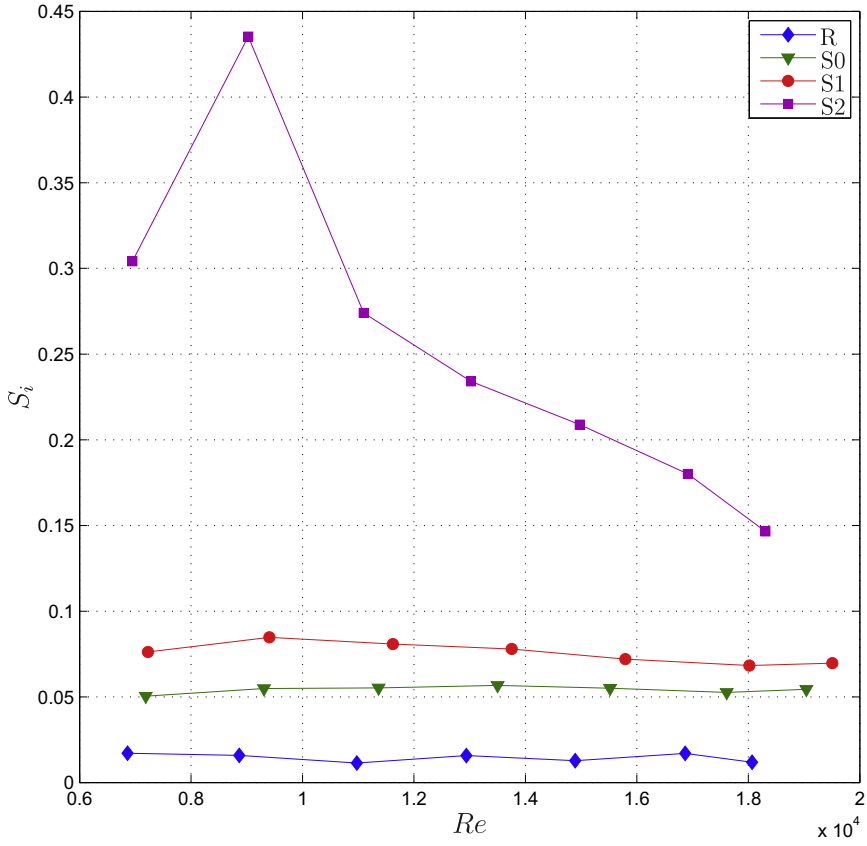

Fig. 3. S_i versus Re for the Cases indicated in the legend.

that takes into account the turbulent thermal conductivity K_t: $K_t = c_p\mu_t/Pr_t$. c_p is the specific heat, μ_t is the turbulent dynamic viscosity and Pr_t is the turbulent Prandtl number;

- regarding the turbulence model, as in [2], the Shear Stress Transport (SST) $k-\omega$ will be used. This selection is motivated by the work presented in [19], where good agreement between numerical and experimental heat transfer results are shown (with the SST $k-\omega$ as the model used), and because the Reynolds number used in this work ranges between around 7000 and 20 000, close to those employed also in [19]. Thus, one closure equation is needed to know the turbulent kinetic energy k and another one to know the specific turbulent dissipation rate ω:

$$\rho\frac{\partial}{\partial x_i}(kV_i) = \frac{\partial}{\partial x_j}\left(\Gamma_k\frac{\partial k}{\partial x_j}\right) + G_k - Y_k, \tag{7}$$

$$\rho\frac{\partial}{\partial x_i}(\omega V_i) = \frac{\partial}{\partial x_j}\left(\Gamma_\omega\frac{\partial \omega}{\partial x_j}\right) + G_\omega - Y_\omega. \tag{8}$$

Γ_k and Γ_ω are the effective diffusivity of k and ω, respectively. G_k and G_ω are the generation of k and ω, respectively, due to mean velocity gradients. And Y_k and Y_ω are the dissipation of k and ω, respectively. To know more about their definition and implementation in Fluent, the reader can consult [20];

- the grid convergence study was carried out with five rectangular stretched meshes with the total nodes ranging from around 13 000 to 60 000. The mesh nodes density is higher near the solid hot wall, the axis, the mixing layer and the nozzle exit;
- to solve efficiently the boundary layer along the solid wall and, therefore, the heat transfer from it, the nearest grid point to the solid hot wall must be as close to the surface as possible to have an $y+$ of unity order. Thus, the maximum of $y+$ will help us to know how good is the mesh under study. The number of nodes of the five meshes, with the maximum value of $y+$ along the solid hot wall indicated in parenthesis, were: 13 041 (8.0), 22 321 (4.0), 30 000 (0.4), 37 901 (0.4) and 60 551 (0.4). The $y+$ values previously indicated were obtained from the numerical simulation of the most unfavorable case studied (see next section): the one with the highest Reynolds number ($Re \simeq 19E3$), the highest swirl intensity (Case S2) and the shortest nozzle-to-wall distance ($H/D = 5$);
- however, the minimum $y+$ obtained in the grid independence process was 0.4, but in 3 different grids, so another magnitude must be used to choose the optimum grid. In our case, the area-weighted average Nusselt number on the solid hot wall was selected.

  On the one hand, the Nusselt number is defined as

$$Nu(r) = \frac{q(r)D}{K\Delta T}, \tag{9}$$

  where $q(r)$ is the total heat flux from the solid hot wall to the fluid and ΔT is the temperature difference between the wall (T_w) and the swirling jet emerging from the nozzle (T_j).

  On the other hand, the area-weighted average Nusselt number on the impinged surface S is defined as

$$Nu_{avg} = \frac{1}{S}\int_S Nu(r)\,dS, \tag{10}$$

  which is a measurement of the dimensionless mean heat transferred from the solid hot wall;
- with the finest grid (60 551 nodes), Nu_{avg} on the solid hot wall only changes ≈1% while the computational time increases by 78% with respect to the grid with ≃38 000 nodes;
- then, the grid chosen as optimum for $H/D = 5$ had $nr \times nz =$ 37 901 nodes (nr and nz are the number of nodes along r and z directions, respectively), with $nr = 251$ non uniform nodes compressed around the axis ($r = 0$) and the mixing layer ($r \simeq D/2$), while $nz = 151$. However, this value was different

depending on the dimensionless nozzle-to-wall distance (for $H/D = 10$, $nz = 201$, and for $H/D = 30$, $nz = 301$), while the grid compression levels were the same than those used in the optimum grid;
- a typical simulation requires about 70E3 iterations to converge;
- around one fifth of the total iterations were done with first order methods, while the remaining iterations were done with the second order schemes PRESTO (PREssure STaggering Option) and QUICK (Quadratic Upwind Interpolation for Convective Kinematics);
- the Pressure–Velocity Coupling were carried out with the SIMPLE (Semi-Implicit Method for Pressure-Linked Equations) scheme; and finally
- the gravity effects have been not taken into account since the inertial forces are much bigger than the gravitational ones, so that the Froude number is much bigger than one.

Although the grid convergence study was carried out to select the optimum grid, as commented previously, to have an idea of the computational uncertainty of the results shown in what follows, two grids, the ones with 30 000 and 37 901 (the optimum) nodes, where used to estimate the discretization error for each Reynolds number when $H/D = 5$ and Case S2 is studied (the cases involving the highest velocities). The discretization error, ϵ, can be estimated using the Richardson extrapolation as

$$\epsilon \simeq \phi_e - \phi_n = K\ h^{\alpha}, \tag{11}$$

where ϕ is any arbitrary magnitude, the subindex e denotes the exact solution of ϕ, while n its numerical approximation, K is an unknown constant, h is a typical cell size of the grid used and α is the order of accuracy of the numerical methods used to obtain ϕ_n. The numerical method used were second order accurate (see above) so $\alpha \approx 2$, so K and, hence, the error ϵ can be estimated with the above mentioned two grids, each of them with different values of h. Once K is obtained, error bars can be associated to the numerical values of ϕ. Since the results are going to be discussed in terms of Nu_{avg} and the stagnation point Nusselt number, i.e. $Nu(r = 0) \equiv Nu_0$, the discretization error of both magnitudes has been calculated and they are plotted in Fig. 4 together with the values of Nu_{avg} and Nu_0. It must be said that since the Nusselt number is calculated along the solid wall, the value of h used in (11) was based on the highest cell next to the wall. As can be seen from Fig. 4, the errors of Nu_{avg} are quite reasonable being all around 1%, while for Nu_0 the errors are higher, especially for high Reynolds numbers and of the order of 5%. Since the Case analyzed is the most unfavorable, we could concluded that, in the worst case, the numerical solution obtained has a computational uncertainty due to the discretization error of about 5%.

4. Results

The aim of this Section is to summarize the results obtained when the heat transfer from a heated solid wall is calculated numerically due to the impingement of a swirling jet generated by a nozzle with moving swirl blades, measured experimentally by LDA and mathematically modeled [1]. The results will be shown in terms of both the area-weighted average Nusselt number, Nu_{avg}, and the stagnation point Nusselt number, Nu_0, calculated along the heated wall. The different subsections will show the effect on the heat transfer of nozzle-to-wall distance, jet swirl intensity and jet Reynolds number. To that end, different and preliminary correlations will be presented.

The section will conclude by presenting new and more general mathematical correlations with the aim of predicting the area-weighted average and stagnation point Nusselt numbers in terms of the different dimensionless parameters governing the problem: Re, S_i, H/D and I_{avg} (precisely defined below). To obtain some of the correlations, the results presented in [2] will be also taken into account, so it will be as general as possible.

4.1. Reynolds number effect

The results related with this effect are summarized in Figs. 5 and 6. They show that, independently of the swirl intensity of the impinging jet, that is, independently of the Case considered, and independently of the nozzle-to-wall distance H/D, almost always that the Reynolds number increases, both the area-weighted average, Nu_{avg}, and stagnation point, Nu_0, Nusselt numbers increase, too. An increase in the inertial force of the impinging jet causes stronger radial wall jets once the impinging jet deviates radially because of the presence of the wall, fact that increases the friction and pressure along the wall and so the wall shear stress and heat transfer coefficients.

In addition, it is remarkable that, once the distance H/D is fixed, Nu_{avg} and Nu_0 almost collapse and increase linearly with Reynolds number independently of the jet swirl intensity (or Case considered). For that reason, Figs. 5 and 6 also include a solid green line representing the linear fitting of the Nusselt values as

$$\left.\begin{matrix} Nu_0 \\ Nu_{avg} \end{matrix}\right\} = \alpha Re + \beta, \tag{12}$$

with $7000 \lesssim Re \lesssim 19\,000$. The slope α and the independent term β of the linear fitting are shown in Table 1. From it, one can observe how the slope of Nu_{avg} decays rapidly with the nozzle-to-wall distance, with a prediction of a very low dependence of Nu_{avg} with Re for higher nozzle-to-wall distances. On the other hand, the slope of Nu_0 seems not to be so dependent of the nozzle-to-wall distance.

4.2. Nozzle-to-wall distance effect

As it has just been pointed out previously, the effect of increasing the distance between the nozzle and the wall is a decrease in the heat transferred from the wall. This applies to both Nu_0 and Nu_{avg}, as can be seen in Fig. 5 and 6, respectively. From them, one can observe how, for a given Reynolds number and Case, an increase in the nozzle-to-wall distance gives as a result a decrease in both Nu_0 and Nu_{avg}, being the value of Nu_0 more dependent on the jet swirl intensity, or Case considered (see next section). Nevertheless, one could go a step further if α and β values of (12) are correlated with H/D to see the effect of both Re and H/D on Nusselt number coefficients. In that case, using the data given in Table 1, the relations obtained for Nu_0 are

$$\begin{aligned} \alpha \cdot 10^3 &= 5.0923 \times (H/D)^{-0.2088}, \\ \beta &= 72.0451 \times (H/D)^{-0.412}, \end{aligned} \tag{13}$$

with an average deviation of around 3.2% for α and 7.7% for β and $5 \leqslant H/D \leqslant 30$. Thus, the correlation of Nu_0 as function only of Re and H/D, and valid for Cases R, S0 and S1, that is, low jet swirl intensity levels, can be written as

$$Nu_0 = 5.0923 \cdot 10^{-3} \times (H/D)^{-0.2088}\ Re + 72.0451 \times (H/D)^{-0.412}, \tag{14}$$

with $7000 \lesssim Re \lesssim 19\,000$ and $5 \leqslant H/D \leqslant 30$.

Fig. 7 shows a comparison between the numerical values of Nu_0 and those given by (14). In the same figure also appears other Nu_0 values experimentally obtained by Bakirci et al. [21] and by Ianiro and Cardone [22], where impinging swirling jets were used to transfer heat from a heated wall, but only those values obtained with the lowest swirl intensity jets have been considered. It must

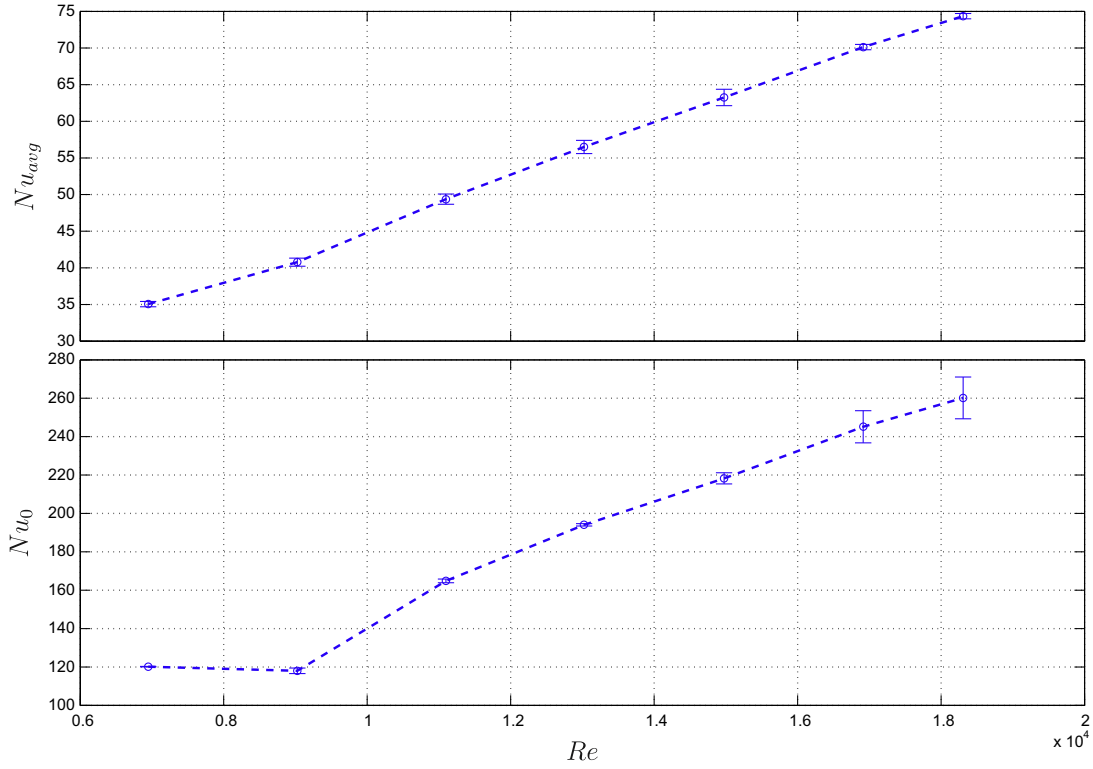

Fig. 4. Nu_{avg} and Nu_0 together with its error bars for all Reynolds number under study when $H/D = 5$ and Case S2.

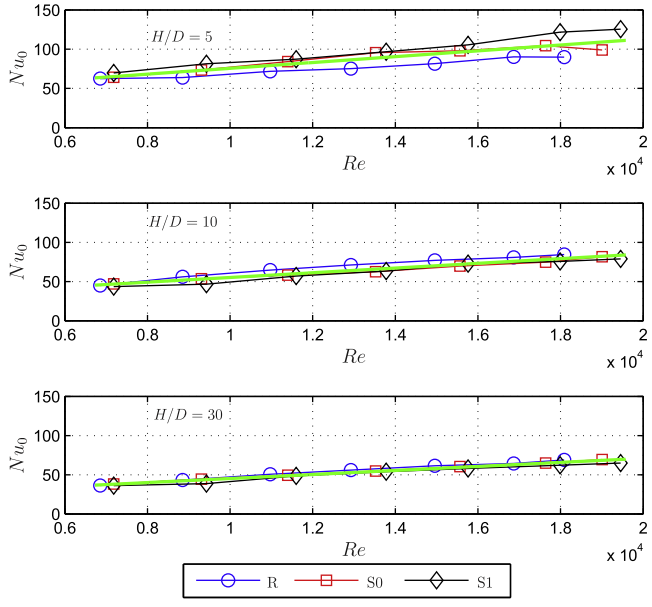

Fig. 5. Variation of Nu_0 with Re for the nozzle-to-wall distances and Cases indicated.

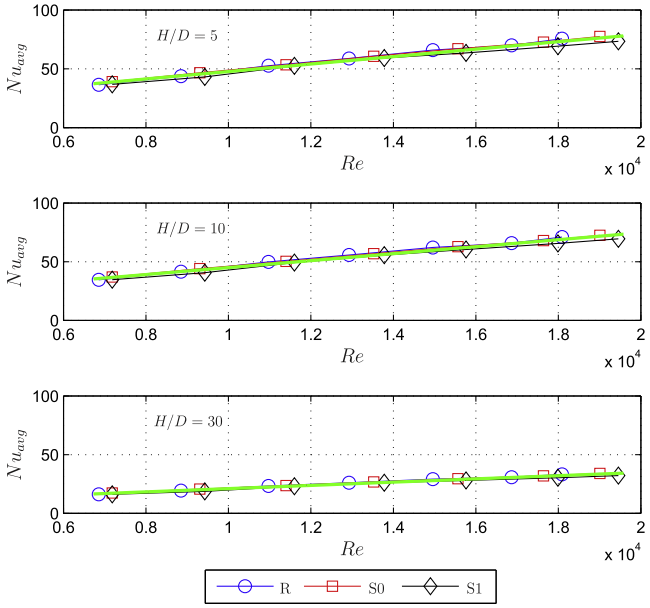

Fig. 6. As in Fig. 5, but for Nu_{avg}.

be noted that in [22] $Re = 28\,000$ and it is out of the range of validity of the correlation. Furthermore, their non-swirling jet results have been considered since their swirl parameter definition is different from the one used here, and it is not clear if their low swirl intensity jets have also low S_i values when (2) is used.

On the other hand, finding a similar correlation for α and β values of Nu_{avg} has not been possible: more complex functions, which depend not only on H/D and Re but also on other dimensionless parameters, seem to be necessary.

Table 1
Slope α and independent term β of the linear least squares fitting shown in Figs. 5 and 6.

$\alpha \cdot 10^3$	$Nu(0,Re)$	$Nu_{avg}(Re)$	β	$Nu(0,Re)$	$Nu_{avg}(Re)$
$H/D = 5$	3.716	3.171	$H/D = 5$	38.40	15.99
$H/D = 10$	3.004	2.988	$H/D = 10$	25.13	15.29
$H/D = 30$	2.574	1.381	$H/D = 30$	19.43	7.21

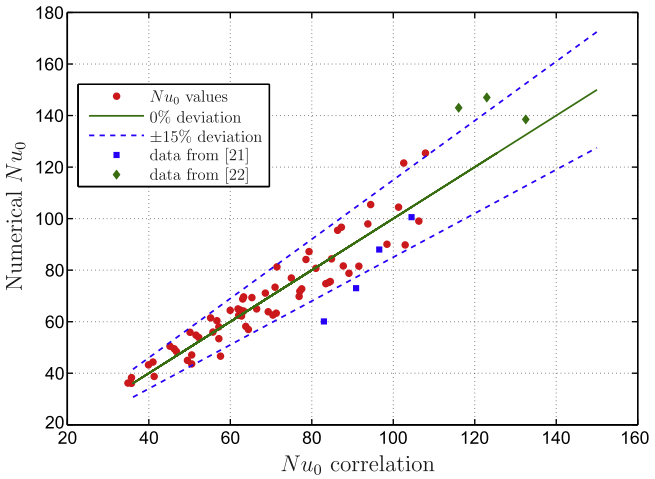

Fig. 7. Confrontation of stagnation point Nusselt number Nu_0 between numerical values and correlation (14) for Cases R, S0 and S1 with low swirl intensity. Nu_0 measured by Bakirci et al. [21] (Re = 20 000, H/D = 6, 8, 10, 14, SJI and 22.5° nozzle configuration) and Ianiro and Cardone [22] (Re = 28 000, H/D = 6, 8, 10 and S = 0) are also included.

4.3. Swirl intensity effect

In order to have a better understanding of the dependence of the heat transferred from the wall to the impinging swirling jet on its swirl intensity, results presented in [2] will be included in the figures mentioned below. Thus, a wider range of swirl intensities will be taken into account.

Figs. 8 and 9 show the variation of Nu_0 and Nu_{avg}, respectively, with the jet swirl parameter S_i for given Reynolds numbers and nozzle-to-wall distances. On the one hand, Fig. 8 shows a small dependence of Nu_0 on S_i when H/D = 5 if only Cases R, S0 and S1 are analyzed. However, the dependence disappears for the other two nozzle-to-wall distances, that is, for $H/D \geqslant 10$, Nu_0 seems not to depend on S_i. If higher jet swirl intensity levels are taken into account (or Case S2 is considered), higher distances are needed in order to have Nu_0 independent of S_i: for H/D = 30, Nu_0 is almost constant for any value of S_i and a given Re number. On the other hand, when the variation of Nu_{avg} with S_i is discussed using Fig. 9, for small to medium nozzle-to-wall distances, that is, H/D = 5, 10, Nu_{avg} does not change with S_i (or Case considered) when Re is almost constant. However, for H/D = 30 and when the highest Re is analyzed, a small increase in Nu_{avg} occurs for Case S2 with respect to Cases R, S0 and S1: an increase in the heat transfer occurs when $Re \simeq 19\,000$ and Case S2 is used.

4.4. Correlations

In this Section, correlations for both Nu_0 and Nu_{avg} as function of the relevant dimensionless parameters of the problem will be presented. They are: the jet Reynolds number Re, the jet swirl intensity S_i, the nozzle-to-wall distance H/D, and the jet area-weighted average turbulent intensity I_{avg}. It is defined as

$$I_{avg} = \frac{2\pi}{\pi(D/2)^2}\int_0^{D/2} I(r) r\,\mathrm{d}r, \tag{15}$$

where $I(r)$ is radial turbulent intensity profile of the jet experimentally measured by means of a LDA system just at the nozzle exit [1] and used as boundary condition in the numerical simulations [2].

On the one hand, regarding the Nu_0 correlation, two functions are proposed: one for swirling jets with low S_i values (<0.1), that is, for Cases R, S0 and S1, and another one for high values of S_i, or Case S2:

(1) when $0.015 < S_i \leqslant 0.1$:

$$Nu_0 = 0.772 \times Re^{0.5644} \times S_i^{0.0246} \times \left(\frac{H}{D}\right)^{-0.2770} \times I_{avg}^{-0.0230}, \tag{16}$$

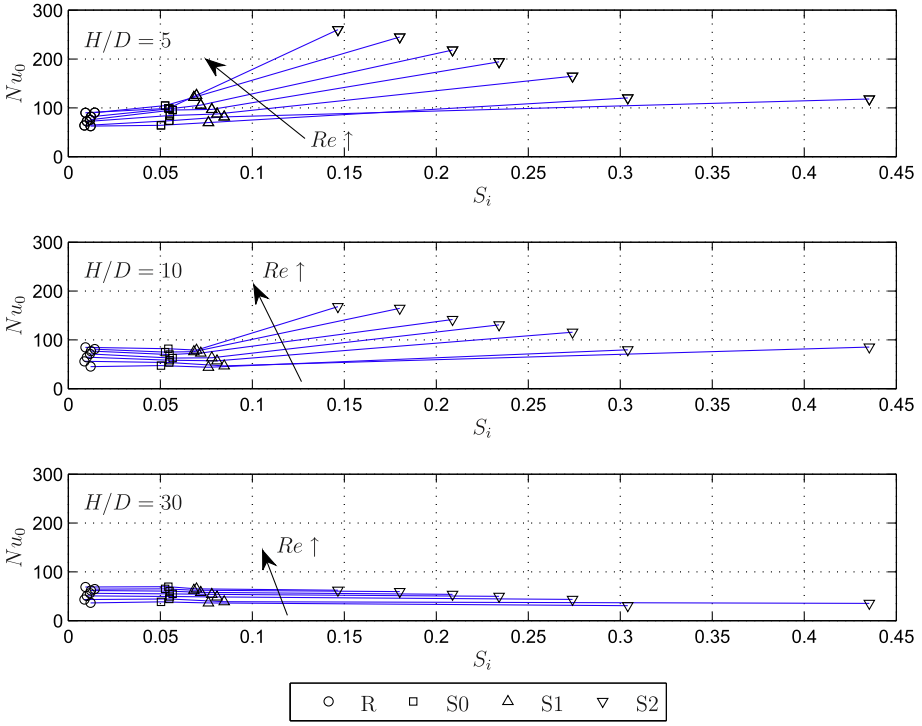

Fig. 8. Nu_0 vs. S_i for the nozzle-to-wall distances and Cases indicated. On each curve, $Re \approx$ constant and it increases as indicated.

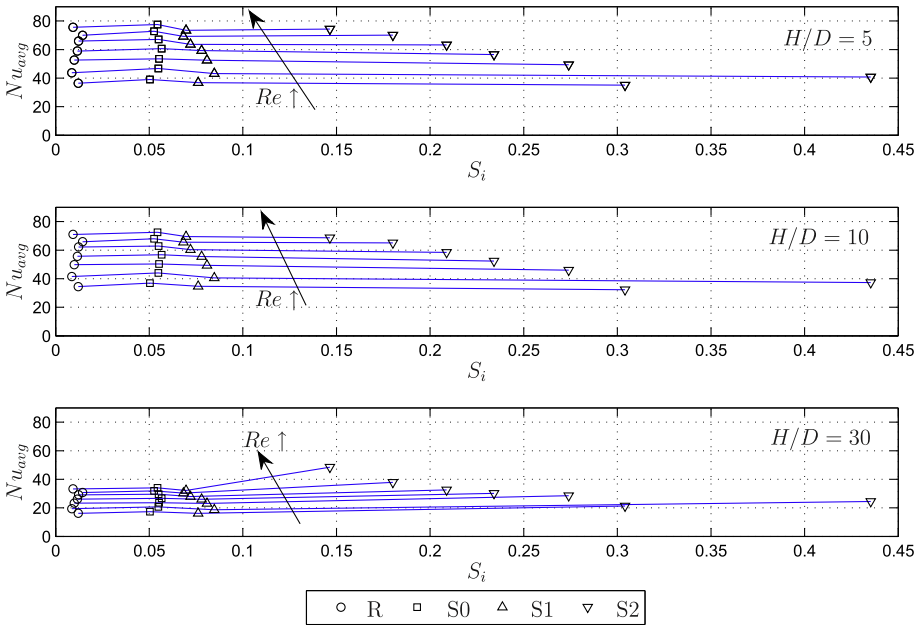

Fig. 9. As in Fig. 8 but for Nu_{avg}.

with $7000 \lesssim Re \lesssim 19\,000$, $5 \leqslant H/D \leqslant 30$ and $9\% \lesssim I_{avg} \lesssim 20\%$;
(2) when $0.1 < S_i < 0.45$:

$$Nu_0 = 0.3246 \times Re^{0.8598} \times S_i^{-0.2414} \times \left(\frac{H}{D}\right)^{-0.7079} \times I_{avg}^{-0.2844}, \tag{17}$$

with $7000 \lesssim Re \lesssim 19\,000$, $5 \leqslant H/D \leqslant 30$ and $20\% \lesssim I_{avg} \lesssim 40\%$.

The average deviation between numerical values and correlations (16) and (17) are of around 7.7% and 7.3%, respectively. Fig. 10 shows how numerical Nu_0 values compare with both correlations (16) and (17). The exponents of S_i and I_{avg} in (16) show that the Nu_0 dependence on the swirl and turbulent jet intensities is very small (for Cases R, S0 and S1), facts that corroborate correlation (14) as the simplest one.

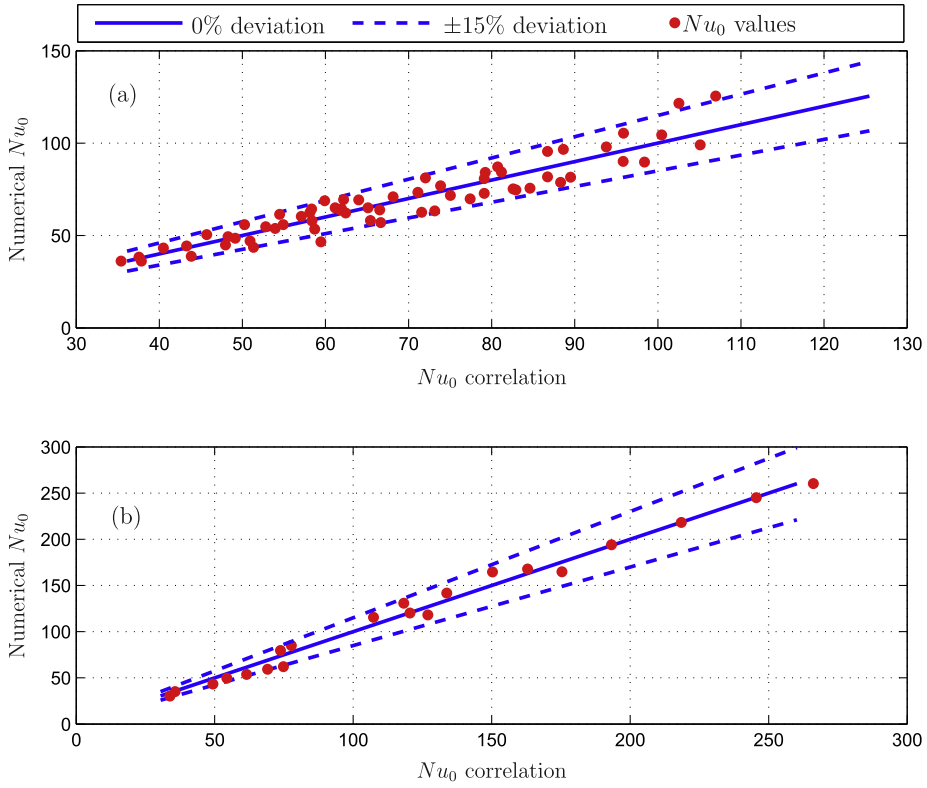

Fig. 10. Confrontation of stagnation Nusselt numbers Nu_0 between numerical values and correlation (16), subfigure (a), and (17), subfigure (b), for different values of Re, S_i, H/D and I_{avg}.

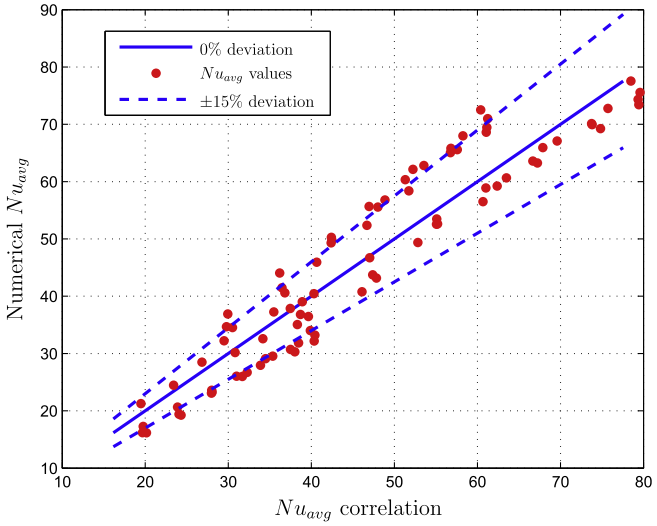

Fig. 11. Confrontation of area-weighted average Nusselt numbers Nu_{avg} between numerical values and correlation (18) for different Re, S_i, H/D and I_{avg}.

On the other hand, regarding the Nu_{avg} correlation, all available data of that magnitude numerically obtained through the numerical simulations carried out have been fitted to a single function (included those presented in [2]):

$$Nu_{avg} = 0.1805 \times Re^{0.6313} \times S_i^{-0.0407} \times \left(\frac{H}{D}\right)^{-0.3780} \times I_{avg}^{0.1132}, \qquad (18)$$

with $7000 \lesssim Re \lesssim 19\,000$, $5 \leqslant H/D \leqslant 30$, $0.015 < S_i < 0.45$ and $9\% \lesssim I_{avg} \lesssim 40\%$.

After the fitting, the errors between the numerical values of Nu_{avg} and the ones given by the correlation have been calculated and an average deviation of around 12% has been obtained. The goodness of the correlation can be checked in Fig. 11, where the confrontation between the values predicted by the correlation and the numerical ones of Nu_{avg} is shown. Again, if the different exponents are checked, a small dependence of Nu_{avg} on S_i and I_{avg} can be observed.

Previously proposed correlations by other authors for both Nu_0 and Nu_{avg} show that both coefficients are proportional to Re and inverse proportional to H/D. A comparison between the exponents here obtained and previous ones can be shown in Table 2. Since previous data are for non-swirling jets, the comparison is carried out with correlations (16) and (18), those with low swirl intensity dependence. It is seen that the exponents of the here proposed correlations are close to previously obtained values.

To conclude this section it must be said that all the coefficients of the correlations have been obtained by non-linear regresion with an interval of confidence of 95%.

5. Conclusion

New correlations to predict the heat transfer coefficients, both the area-weighted average Nusselt number Nu_{avg} and the stagnation point Nusselt number Nu_0, from a impinged heated wall by turbulent swirling jets have been proposed as function of the dimensionless parameters governing the problem: the jet Reynolds number Re, the jet swirl intensity S_i, the nozzle-to-wall distance H/D, and the jet area-weighted average turbulent intensity I_{avg}. To that end, a number of turbulent, steady and axisymmetric numerical simulations of an incompressible fluid have been carried out by means of the commercial code Fluent. The velocity profiles used as boundary condition to model the swirling jet had been previously measured and modeled in [1], where the velocity components of the jet emerging from a swirl generator nozzle with swirl blades were measured by a LDA system and fitted to mathematical models. Depending on the rotation of the swirl blades, jets with different swirl intensities can be generated by the nozzle. The heat transferred to the impinging swirling jet when the blades are rotated the maximum angle (Case S2) was previously presented in [2] and its Nu_{avg} and Nu_0 data have been taken into account in this work to get some correlations. Those Nusselt values, together with the ones obtained in this work for other nozzle configurations, have allowed to present the different correlations above mentioned. While for Nu_{avg} one correlation has been proposed for any combination of the governing parameters and nozzle configuration, for Nu_0 two are needed, depending on the nozzle configuration (or jet swirl intensity): one for Cases R, S0 and S1 (or jets with low swirl intensity), and another one only for Case S2 (or jets with medium swirl intensity). From the proposed correlations, one can easily see that:

1. both Nu_0 and Nu_{avg} always increase when Re increase: $\sim Re^m$, $m > 0$;
2. both Nu_0 and Nu_{avg} always decrease when H/D increase: $\sim \left(\frac{H}{D}\right)^m, m < 0$;
3. with regard to the jet swirl intensity:
   (a) Nu_{avg} slightly decreases when S_i increases: $\sim S_i^m, m < 0$;
   (b) Nu_0 slightly increases with S_i, if $S_i < 0.1$: $\sim S_i^m, m > 0$; while
   (c) Nu_0 decreases when S_i increases, if $S_i > 0.1$: $\sim S_i^m, m < 0$.

In addition to this, a simpler correlation for Nu_0 has been proposed depending only on Re and H/D, when $S_i < 0.1$, where the above mentioned dependence of Nu_0 on Re and H/D is also confirmed; and.

4. finally, with regard to the jet area-weighted average turbulent intensity:
   (a) Nu_{avg} increases when I_{avg} increases: $\sim I_{avg}^m, m > 0$; and
   (b) Nu_0 decreases when I_{avg} increases: $\sim I_{avg}^m, m < 0$, being little the dependence when $S_i < 0.1$.

The proposed correlations are then ready to be used as a tool to estimate the heat transfer coefficients from heated solid walls under the impingement of swirling jets generated by nozzles with

Table 2
Value of the exponents in different Nu_0 and Nu_{avg} correlations.

Nu_0 data set	[8]	[9]	[10]	[11]	Eq. (16)
Re exponent	0.54	0.4:0.6	0.5:0.53	0.67:0.701	0.5644

Nu_{avg} data set	[10]	[12]	[13]	[14]	[15]	[16]	Eq. (18)
Re exponent	0.68	0.5	0.62	0.574	0.696	0.55	0.6313

Data set	[10]	[11]	[15]	[17]	Eq. (16)	Eq. (18)
H/D exponent	−0.191:−0.288	−0.182:−0.38	−0.20	−0.22	−0.2770	−0.3780

rotating swirl blades. They are also thought to be valid to have an idea of how jet governing parameters will affect the heat transfer in any engineering application where swirling jets are involved.

Acknowledgments

The author thanks Nicolás Campos Alonso, who was the responsible for taking the LDA measurements at the laboratory of the Fluid Mechanics Group at the University of Málaga.

All the numerical simulations were carried out in the computer facility "Taylor" at the Computational Fluid Dynamic Laboratory of the Fluid Mechanic Group at the University of Málaga.

References

[1] J. Ortega-Casanova, N. Campos, R. Fernandez-Feria, Experimental study on sand bed excavation by impinging swirling jet, Journal of Hydraulic Research 49 (5) (2011) 601–610.
[2] J. Ortega-Casanova, Numerical simulation of the heat transfer from a heated solid wall to an impinging swirling jet, in: Amimul Ahsan (Ed.), Two Phase Flow, Phase Change and Numerical Modeling, InTech, 2011, ISBN 978-953-307-584-6. http://www.intechopen.com/books/two-phase-flow-phase-change-and-numerical-modeling/numerical-simulation-of-the-heat-transfer-from-a-heated-solid-wall-to-an-impinging-swirling-jet.
[3] B. Han, R.J. Goldstein, Jet-impingement heat transfer in gas turbine systems, Ann. NY. Acad. Sci. 934 (2001) 147–161.
[4] B.R. Hollworth, M. Durbin, Impingement cooling of electronics, ASME J. Heat Transfer 114 (1992) 607–613.
[5] S. Roy, K. Nasr, P. Patel, B. AbdulNour, An experimental and numerical study of heat transfer off an inclined surface subject to an impinging airflow, Int. J. Heat Mass Transfer 45 (2002) 1615–1629.
[6] D. Babic, D.B. Murray, A.A. Torrance, Mist jet cooling of grinding processes, Int. J. Machine Tools Manu. 45 (2005) 1171–1177.
[7] N. Zuckerman, N. Lior, Jet impingement heat transfer: physics, correlations, and numerical modeling, in: J. Hartnett, Y.I. Cho, A. Bar-Cohen (Eds.), Advances in Heat Transfer, Elsevier Inc, New York, 2006, pp. 565–631.
[8] T.L. Chan, C.W. Leung, K. Jambunathan, S. Ashforth-Frost, Y. Zhou, M.H. Liu, Heat transfer characteristics of a slot jet impinging on a semi-circular convex surface, Int. J. Heat Mass Transfer 45 (2002) 993–1006.
[9] J.-Y. San, M.-D. Mao-De Lai, Optimum jet-to-jet spacing of heat transfer for staggered arrays of impinging air jets, Int. J. Heat Mass Transfer 44 (2001) 3997–4007.
[10] D. Lytle, B. Webb, Air jet impingement heat transfer at low nozzle-plate spaces, Int. J. Heat Mass Transfer 37 (1994) 1687–1697.
[11] A.K. Mohanty, A.A. Tawfek, Heat transfer due to a round jet impinging normal to a flat surface, Int. J. Heat Mass Transfer 36 (1993) 1639–1647.
[12] M. Behnia, S. Parneix, Y. Shabany, P.A. Durbin, Numerical study of turbulent heat transfer in confined and unconfined impinging jets, Int. J. Heat Fluid Flow 20 (1999) 1–9.
[13] B. Merci, E. Dick, Heat transfer predictions with a cubic $k-\epsilon$ model for axisymmetric turbulent jets impinging onto a flat plate, Int. J. Heat Mass Transfer 46 (2003) 469–480.
[14] H. Martin, Heat and mass transfer between impinging gas jets and solid surfaces, Adv. Heat Transfer 13 (1977) 1–60.
[15] M.Y. Wen, K.J. Jang, An impingement cooling on a flat surface by using circular jet with longitudinal swirling strips, Int. J. Heat Mass Transfer 46 (2003) 4657–4667.
[16] X. Yan, A preheated-wall transient method using kiquid crystals for the measurement of heat transfer on external surfaces an in ducts, PhD Thesis, University of California, Davis, 1993.
[17] A.A. Tawfek, Heat transfer and pressure distributions of an impinging jet on a flat surface, Heat Mass Transfer 32 (1996) 49–54.
[18] N.A. Chigier, A. Chervinsky, Experimental investigation of swirling vortex motion in jets, J. Appl. Mech. 34 (1967) 443–451.
[19] B. Sagot, G. Antonini, A. Christgen, F. Buron, Jet impingement heat transfer on a flat plate at a constant wall temperature, Int. J. Therm. Sci. 47 (2008) 1610–1619.
[20] Fluent 6.2 user's guide. Fluent Incorporated, Centerra Resource Park, 10, Cavendish Court, Lebanon (NH) 03766 USA, 2005.
[21] K. Bakirci, K. Bilen, Visualization of heat transfer for impinging swirl flow, Exp. Therm. Fluid Sci. 32 (2007) 182–191.
[22] A. Ianiro, G. Cardone, Heat transfer rate and uniformity in multichannel swirling impinging jets, Appl. Therm. Eng. (2011). http://dx.doi.org/10.1016/j.applthermaleng.2011.10.018.